Iranian Journal of Materials Forming 8 (2) (2021) 22-34

IJMF

Online ISSN: 2383-0042

Iranian Journal of Materials Forming

Journal Homepage: http://ijmf.shirazu.ac.ir

Research Article

Investigation of Stress Concentration Factors for Functionally Graded Hollow Tubes with Curved Edges under Torsion

Z. Ebrahimi* and S. Negahban

Mechanical Engineering Department, Payame Noor University, Iran

ARTICLE INFO

Article history:

Received 8 January 2021
Reviewed 3 February 2021
Revised 18 February 2021
Accepted 1 March 2021

Keywords:

Hollow tube
FGMs
Stress concentration
Torsion
Shear stress

ABSTRACT

In this paper, a finite element (FE) model is developed to calculate stress concentration factors of functionally graded (FG) hollow tubes under torsion. First, the shear stresses in FG hollow tubes with curved edges are investigated for different curvature radius of the cross-section corners. Next, stress concentrations are evaluated at low curvature parts of the cross-sections. Due to stress concentrations in low curvature regions, more considerable shear stresses are obtained. FE results are compared with the results of an analytical method for analysis of the torsion of hollow tubes to verify the computational approaches. Except for the points of stress concentrations, in other regions, an excellent agreement is found between analytical and FE results. Therefore, in stress concentration regions, regarding the error of analytical formula in stress analysis, some correction factor is presented. These stress concentration factors are calculated for a variety of curvature radius and cross-section thicknesses. Applying the presented factors, the proposed analytical formula can be used for stress evaluations, even at stress concentration regions. Finally, the effects of changing the volume fraction of the constituent phases are investigated for a range of curvature radius of cross-section corners.

1. Introduction

Complex torsion problems have become a serious concern to many researchers in the area of elasticity theory. Due to the high strength to mass ratio of hollow tubes, researchers have focused more on the torsion of hollow members. Inhomogeneous hollow rods have spatially varying mechanical and thermal properties. This gradual change of material properties can be tailored to meet desired application requirements. Such materials, which are mostly composed of two or more constituents with gradually varying volume fraction distribution, are called functionally graded materials (FGMs).

Recently, stress analysis of hollow functionally graded (FG) structures has attracted many researchers. Studies on torsion of hollow structures with spatially varying properties have led to an accurate analytical solution for stress analysis of circular, ellipsoidal, and polygonal hollow tubes. Chandra et al. tested symmetric and non-symmetric epoxy composite rods of rectangular cross-section under flexural, torsional, and axial loads [1]. Savoia and Tullini investigated the torsional response of inhomogeneous multilayered composite beams [2]. Horgan and Chan studied torsion of FG elastic bars using Prandtl's stress function [3]. Mejak designed optimal shapes for hollow prismatic bars in

* Corresponding author
E-mail address: z.ebrahimi@pnu.ac.ir (Z. Ebrahimi)
https://doi.org/10.22099/ijmf.2021.39443.1175

torsion [4]. The governing equations of the torsion problem of hollow tubes with polygon shapes are formulated in terms of Prantl's stress function by Hematiyan and Doostfatemeh [5]. This formulation is later extended to torsion of hollow tubes with straight and circular edges [6]. Using the same stress function, Arghavan and Hematiyan presented an analytical formula for the torsion of FG hollow tubes with arbitrary cross-sections [7]. They assumed that the shear modulus of rigidity varies through the thickness of the tube, based on a power-law distribution. Ecsedi presented analytical solutions for non-homogenous hollow solid cylinders [8]. Golami Bazehhour and Rezaeepazhand presented a method for analyzing the torsion of non-homogeneous tubes with arbitrary cross-sections [9]. Bayat et al. investigated FG hollow cylinders under torsional load considering a radial variation of material properties [10]. Talebanpour and Hematiyan also studied the torsion of piezoelectric hollow bars with arbitrary cross-sections [11]. Barretta et al. investigated torsion of two-phase random composite beams with simple and multiply connected cross-sections [12].

Stress analysis of cracked hollow cylinders made of FGMs is performed by Eshraghi et al. for thermomechanical loading conditions [13]. The torsional deformations of hollow truncated conical cylinders made of FGMs are studied by Batra and Nie [14]. Wang et al. performed stress analysis of arbitrary FG layered hollow cylinders under arbitrary loading conditions [15]. Stress analysis of cracked hollow cylinders made of FGMs is performed by Ghasemi and Noroozi [16] for torsional loading. Nikbakht et al. reviewed optimization-related research of FG structures, including hollow tubes and tubes filled with foams [17].

In all of the mentioned studies, the effect of stress concentration on curved edges at a low radius of curvature is neglected. Nigrelli and Mariotti calculated the stress concentration of coaxial shafts under torsion [18]. Stress concentration factors (SCFs) formed under tension, bending, and torsion have been considered for cylindrical components [19]. The calculation of SCFs in the mentioned literature, has been performed for isotropic components. To the best of the author's knowledge, determination of SCFs for FG tubes under torsion has not been presented in the literature.

In this paper, a finite element (FE) model has been developed to calculate SCFs of FG hollow tubes under torsion. The torsion problem of FG hollow tubes with curved edges at a considerably low curvature radius of the cross-section corners has not been studied yet. First, the shear stresses in FG hollow tubes with curved edges are investigated for different curvature radius of the cross-section corners. The plots of SCFs versus curvature radius of the corners are obtained for a variety of the cross-section thicknesses. The FE results are compared with the analytical results presented in Ref. [7] for model validation. Finally, the effects of constituent volume fractions are investigated for a range of radius of curved segments.

With the aim of the presented results, SCFs for other values of curvature radius can be obtained by interpolation. Using these SCFs, the analytical formula of Ref. [7], can also be applied to the stress concentration regions for both rounded square and flattened tube cross-sections made of FGMs, with reasonable accuracy.

2. Materials and Methods

2.1. Analytical solution

The stress analysis of hollow tubes with polygon shapes under torsion are formulated in terms of Prantl's stress function in Ref. [5]. This formulation is then extended to torsion of hollow tubes with straight and circular edges [6]. Later, an analytical formula for torsion of FG hollow tubes with arbitrary cross-sections is presented by Arghavan and Hematiyan [7].

Here, the proposed analysis of Ref. [7] is adopted to evaluate the SCFs of FG hollow tubes with curved edges under torsion. First, the general relations governing the torsion of non-homogenous materials are discussed. The governing equations and boundary conditions of this problem are given in equations (1) to (3),

$$\vec{\nabla} \cdot \left(\frac{1}{G} \vec{\nabla} \phi \right) = -2\alpha \tag{1}$$

$$\int_{\Gamma_1} \frac{\tau}{G} ds = 2\alpha A_{\Gamma_1} \quad (2)$$

$$T = 2\iint_R \phi dxdy + 2\phi_1 A_{\Gamma_1} \quad (3)$$

In the above relations, ϕ is the Prandtl's stress function, α is the twist angle per unit length, τ is the total shear stress, and T is the input torque. A_{Γ_1} describes the area enclosed by the inner boundary, while n is the normal unit vector to the constant ϕ contour. The boundary conditions on the outer and inner boundaries are $\phi = 0$ and, $\phi = \phi_1$, respectively. The value of ϕ_1 satisfies Eq. (2). The shear stress is obtained at each point of the cross-section by $\tau = -d\phi / dn$.

The material properties of the constituent phases in FGMs, change continuously along the direction of cross-section thickness. Here, the FG material is composed of two constituent phases, with a shear modulus variation designed according to the power-law distribution with an exponent k. G_0 is the shear modulus of the material at the outer boundary and G_i is the one at inner boundary.

Now, considering constant thickness for all parts of the FG hollow tube, the proposed cross-section will be divided into straight and curved segments. The shear modulus is obtained at each point in the straight and curved segments as Eq. (4) and Eq. (5), respectively.

$$G = (G_i - G_o)\left(\frac{x'}{t}\right)^k + G_o \quad (4)$$

$$G = (G_i - G_o)\left(\frac{r_2 - r}{t}\right)^k + G_o \quad (5)$$

where k is the volume fraction of the material at the outer boundary and, t is the cross-section thickness. The local Cartesian coordinate system, x'-y', is used for the straight segments, where x' is perpendicular to the segment length toward the inner surface. For the curved segments, the polar coordinate system rθ is defined, where it's center is the center of the arced segment.

Substituting equations (4) and (5) in Eq. (2) and using $\tau = -d\phi / dn$, the shear stress relations for the straight and curved segments of the cross-section along the thickness direction, are presented in Eq. (6) and (7),

$$\tau_i(x') = -2\alpha x' G_o + C_1 G_o - \frac{2\alpha(G_i - G_o)}{t^k} x'^{k+1} + \frac{C_1(G_i - G_o)}{t^k} x'^k \quad (6)$$

$$\tau_j(r) = \frac{\alpha r(G_i - G_o)}{t^k}(r_{2j} - r)^k - \frac{G_o C_{2j}}{r} + \alpha r G_o - \frac{C_{2j}(G_i - G_o)}{t^k r}(r_{2j} - r)^k \quad (7)$$

where r_{1j} and r_{2j} are the inner and outer radius of the jth curved segment and R_j is it's averaged radius. The constant coefficients of the above relations are defined in terms of shear flow according to Ref. [7] as presented in Eq. (8) and Eq. (9),

$$C_1 = \frac{\left(\frac{q}{t} + \alpha G_o t + \frac{2\alpha(G_i - G_o)}{k+2} t\right)}{\left(G_o + \frac{G_i - G_o}{k+1}\right)} \quad (8)$$

$$C_{2j} = \frac{\left(\frac{\alpha(G_i - G_o)}{(k+1)(k+2)}\left((k+1)r_{1j} + r_{2j}\right) + \alpha G_o R_j - \frac{q}{t}\right)}{\left(\frac{G_o}{t}\ln\left(\frac{r_{2j}}{r_{1j}}\right) + \frac{(G_i - G_o)}{t^{k+1}} I_j\right)} \quad (9)$$

in which I_j is obtained from Eq. (10),

$$I_j = \int_{r_{1j}}^{r_{2j}} \frac{(r_{2j} - r)^k}{r} dr \quad (10)$$

The relation between the angle of twist per unit length (α) and the shear flow (q) is given in Eq. (11),

$$q = \frac{2A_{\Gamma_1} - \sum_j p_j + \left(2t - \frac{\left(G_o t + \frac{2(G_i - G_o)t}{(k+2)}\right)}{\left(G_o + \frac{(G_i - G_o)}{k+1}\right)}\right)\sum_i l_i}{\sum_j q_j + \frac{1}{t\left(G_o + \frac{(G_i - G_o)}{k+1}\right)}\sum_i l_i}\alpha \quad (11)$$

in which the constants given in Eq. (12) and Eq. (13) are used [7],

$$p_j = r_{1j}^2 \beta_j - \beta_j \frac{\left(\frac{(G_i - G_o)}{(k+1)(k+2)}\left((k+1)r_{1j} + r_{2j}\right) + G_o R_j\right)}{\left(\frac{G_o}{t}\ln\left(\frac{r_{2j}}{r_{1j}}\right) + \frac{(G_i - G_o)}{t^{k+1}} I_j\right)} \quad (12)$$

$$q_j = \frac{\beta_j}{G_o \ln\left(\frac{r_{2j}}{r_{1j}}\right) + \frac{(G_i - G_o)}{t^k} I_j} \quad (13)$$

Then, using the above analytical formula, the shear stresses versus curvature radius of curved segments are investigated for two types of FG hollow tubes for a variety of cross-section thickness and later, the corresponding SCFs are evaluated.

2.2. FE solution

An FE model is developed to calculate SCFs of FG hollow tubes with curved edges using Ansys software. The FE results are then compared to the analytical solutions of the previous section. Two types of cross-sections are examined. The rounded square cross-section consists of four straight pieces and four curved segments (Fig. 1(a)), while the flattened tube section has two straight and two curved segments (Fig. 1(b)).

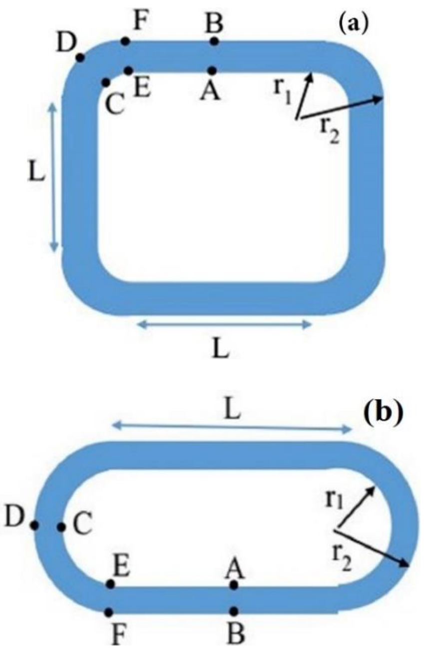

Fig. 1. (a) Rounded square cross-section, (b) and flattened tube cross-section.

In Fig. 1, three points at inner boundary, namely C, E and A, and points D, F and B at the outer boundary are established. The normalized shear stress at point E is equal to the average value of the normalized shear stress at points A and C. The inner radius is r_1 and, r_2 is the outer radius of both examples.

According to equations (6) and (7), the shear stress, in the thickness direction, is expressed in terms of α. Since the shear stress has a linear relationship with α, we define the normalized shear stress as $\tau / 2\alpha$.

The FG material has two constituent phases and, the shear modulus is regarded as varying along the thickness direction based on the power-law distribution. The inner surface of the FG hollow tube is metal-rich with $G_i = 77\,\text{GPa}$, while the outer boundary is ceramic-rich with $G_o = 25.5\,\text{GPa}$.

The FE model mesh is shown in Fig. 2, where only 1/8 of the rounded square cross-section (Fig. 2(a)) and 1/4 of the flattened tube cross-section (Fig. 2(b)) are modeled due to the model symmetries. This significantly reduces the number of elements and nodes of the FE model, which in turn reduces the computational costs. The number of the elements through the thickness is chosen as 32 according to a mesh study, which is performed before stress analysis. The length of the straight segment for both cross-sections is L=100 mm.

The thermal analysis of the Ansys software is applied here to model the torsion problem, recalling that the torsion and two-dimensional heat transfer governing equations are identical. The temperature in the heat transfer problem is the same as the Prandtl's stress function in the torsion problem. Hence, the temperature is set to zero on the outer boundary and an unknown value on the inner boundary.

After performing the FE simulations, the constant ϕ contours are shown in Fig. 3 for an averaged radius of R=50 mm, cross-section thickness of t=20 mm and, k=1. The constant ϕ contour lines are parallel to the boundary of the cross-sections.

Using the proposed FE model, the normalized shear stresses on points A, E and C on the inner boundary and points B, F and D on the outer boundary are calculated for different values of the curvature radius and cross-section thickness. Then, the FE results are compared with those of the analytical solution presented in previous sub-sections. Note that in analytical model, the normalized shear stress at point E is set to the averaged value of shear stress at points A and C. Similarly, shear stress at point F is equal to the averaged value of shear stress at points D and B.

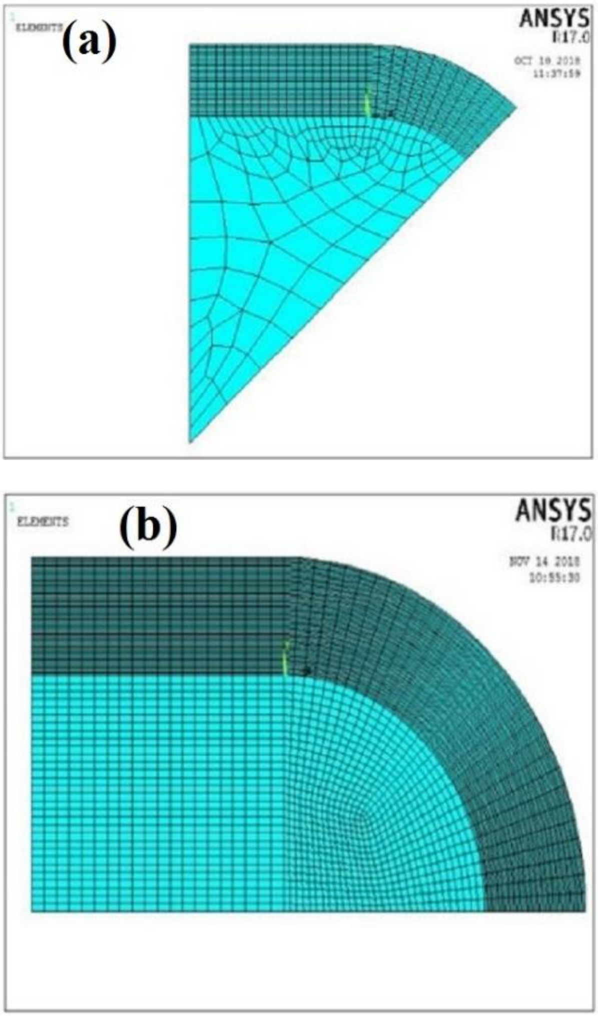

Fig. 2. The FE model, (a) Rounded square and, (b) Flattened tube cross-sections.

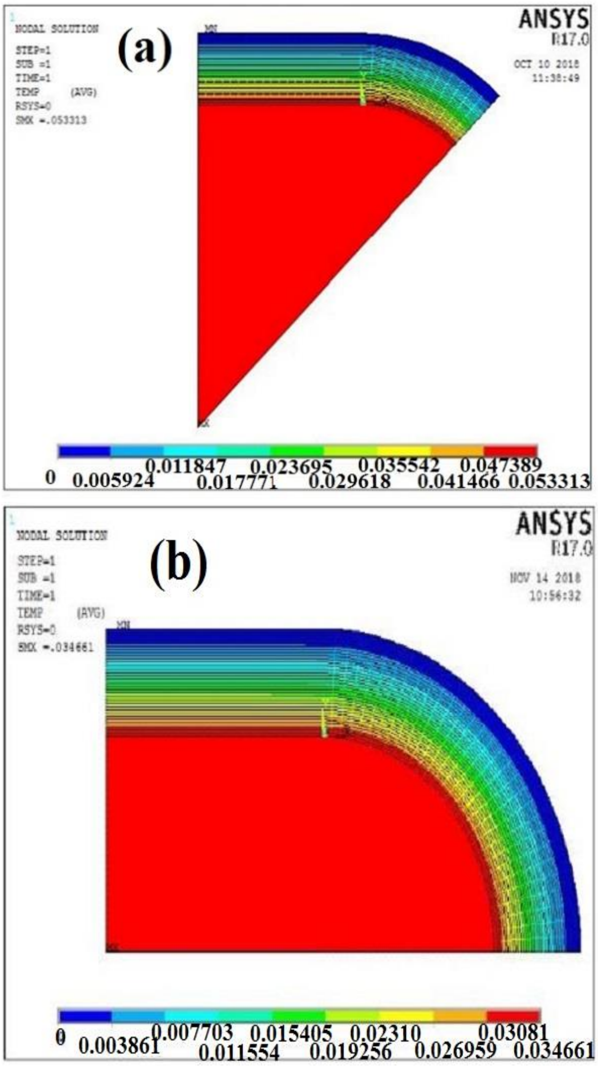

Fig. 3. The constant ϕ contours for R=50 mm, t=20 mm and k=1. (a) Rounded square cross-section, (b) flattened tube cross-section.

3. Results and discussions

3.1. Effects of curvature radius on normalized shear stress for k=1

3.1.1. Rounded square cross-section

The effects of the radius of curvature variations on shear stress in a rounded square cross-section with a thickness of 5 mm and k=1, are investigated on both the inner and outer boundaries of the cross-section. The normalized shear stress versus averaged curvature radius are shown in Fig. 4 and Fig. 5 on inner and outer boundaries, respectively. It can be seen that there is a good agreement between the stress values calculated by the FE method and those of the proposed analytical method.

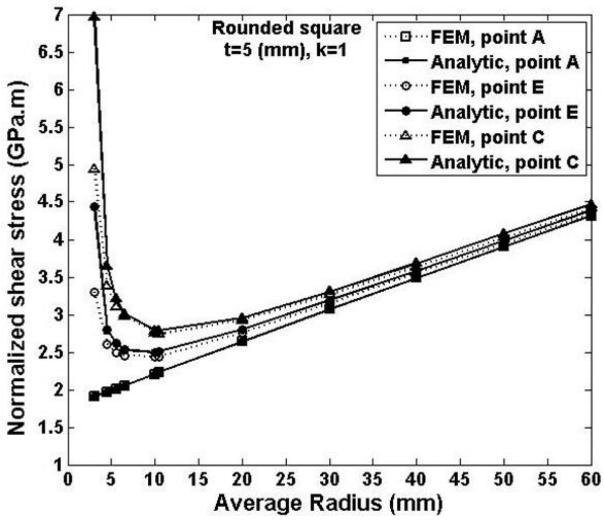

Fig. 4. Normalized shear stress at points C, E and A on inner boundary of the rounded square cross-section with t=5 mm and k=1.

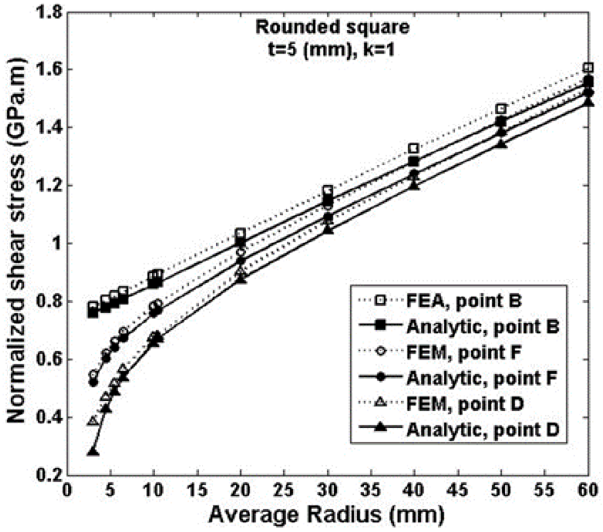

Fig. 5. Normalized shear stress at points D, F and B versus curvature radius for t=5 mm and k=1.

However, at points C and E, the normalized shear stress has a decreasing trend from R=3 to R=10 mm and after that, it returns to its usual increasing trend. The difference between the analytical and FE results at points C and E are presented in Table 1, as an error of the analytical solution. By comparing the results of the accurate FE method with those of the proposed analytical method at points C and E (Table 1), we find that the accuracy of the analytical formula is not adequate at stress concentration regions. Therefore, in the present article, some coefficients are evaluated to correct the analytical formula. These SCFs are given in Section 3.3.

Similar simulations have been performed for rounded square hollow tube cross-sections with thicknesses of 10, 20 and 40 mm.

For the rounded square cross-section with a thickness of 10 mm, according to Figures 6 and 7, at point A on the inner boundary and points B, F and D on the outer boundary, by increasing the radius of curvature, the normalized shear stress has increased uniformity. There is a slight difference between the FE and analytical solutions at these points. However, at points C and E, the amount of normalized shear stress has decreased in low curvature radiuses, which is due to the stress concentration on the corners of the cross-section. As the radius of curvature increases, the stress concentration decreases, and shear stresses return to the usual increasing trend.

Table 1. Error of the calculated analytical normalized shear stress at points C and E for t=5 mm and k=1

Relative Error Percent (%)			
R (mm)	r_1 (mm)	E	C
3	0.5	34.253	40.804
4.5	2	7.660	7.917
5.5	3	5.106	3.688
6.5	4	3.273	1.158
10	7.5	2.363	1.222
10.5	8	2.665	1.702
20	17.5	1.588	1.111
30	27.5	1.338	1.104
40	37.5	1.124	1.431
50	47.5	1.220	1.106
60	57.5	1.177	1.105

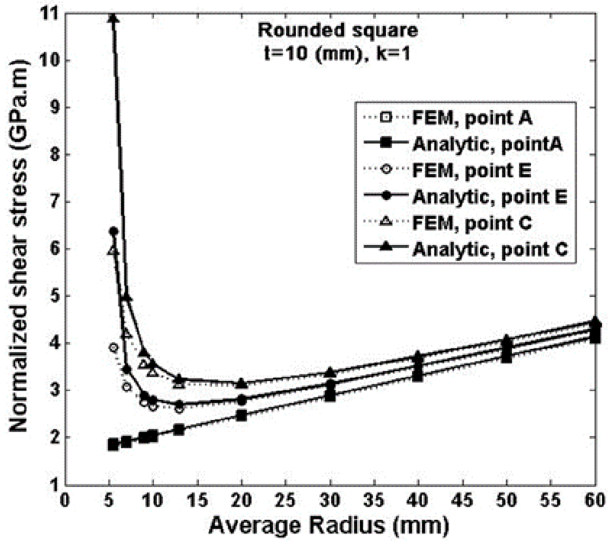

Fig. 6. Normalized shear stress at points C, E and A versus curvature radius with t=10 mm and k=1.

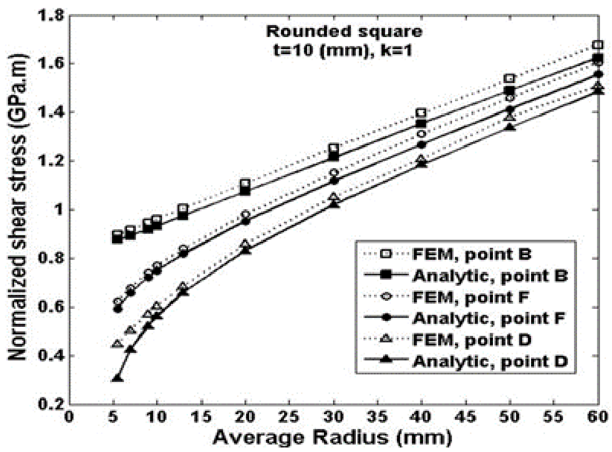

Fig. 7. Normalized shear stress at points D, F and B versus curvature radius with t=10 mm and k=1.

Figures 8 and 9 illustrate the normalized shear stress versus curvature radius on the inner and outer boundaries for a cross-section of 20 mm thickness.

According to Figures 8 and 9, it is clear that the amount of normalized shear stress for the rounded square cross-section with a thickness of 20 mm, on the outer boundary points and point A on the inner boundary, have a uniform upward trend by increasing curvature radius. Due to the stress concentration on the corners at low curvature points C and E, the normalized shear stress decreases from R=10.5 to R=20 mm. Hence, the stress concentration decreases by increasing the curvature radius. After that, the variation of shear stress will ascend as the radius of curvature increases.

The results of the shear stress evaluation for t = 40 mm are shown in Figures 10 and 11 for the inner and outer boundaries. For the rounded square cross-section with a thickness of 40 mm, although the section is relatively thick, an increasing trend is observed in plots of shear stress versus curvature radius at point A on inner and B, F and D on the outer boundaries. However, at the corners, points C and E, the stress concentration causes a decrease of shear stress as the curvature radius increases to 40 mm. After that, it returns to its usual increasing trend.

Moreover, in the stress concentration regions, the difference between analytical and FE results is significant. Therefore, a correction factor for the analytical solution will be introduced in section 3.3.

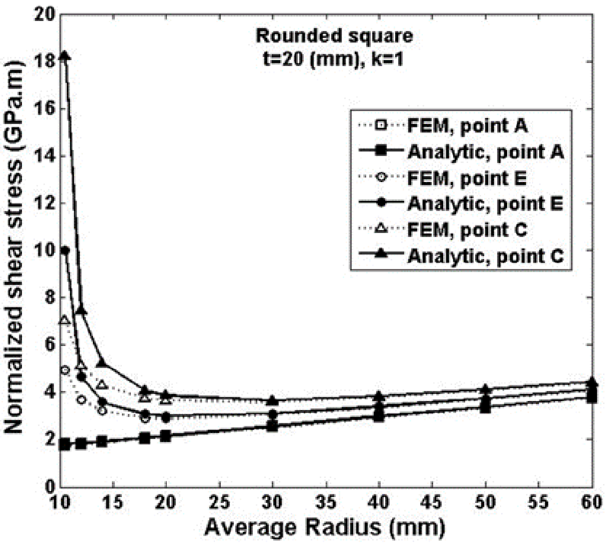

Fig. 8. Normalized shear stress at points C, E and A versus curvature radius with t=20 mm and k=1.

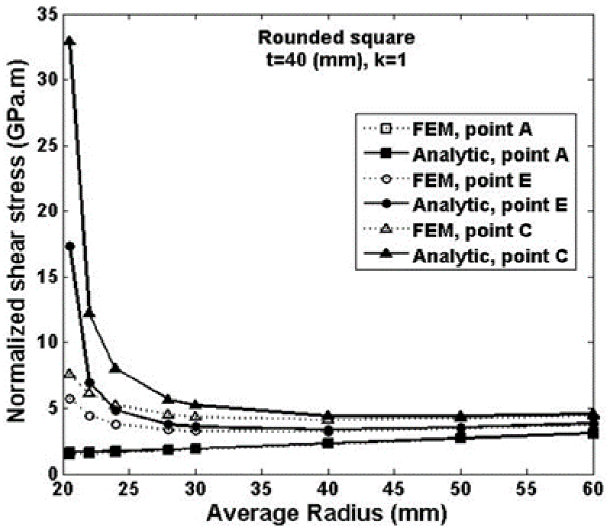

Fig. 10. Normalized stress at points C, E and A versus curvature radius with t=40 mm and k=1.

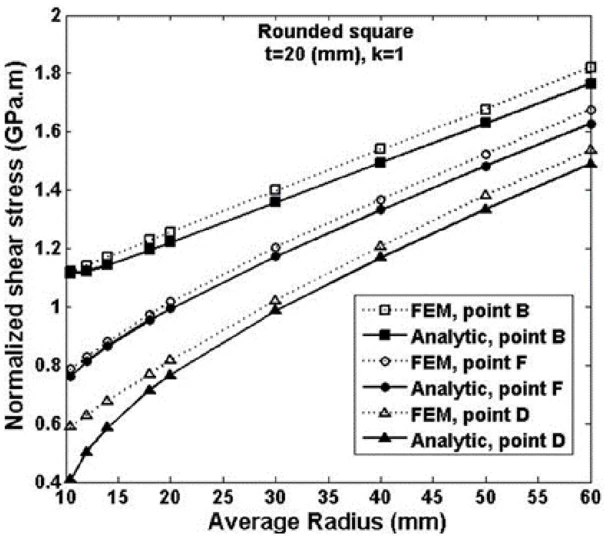

Fig. 9. Normalized shear stress at points D, F and B versus curvature radius with t=20 mm and k=1.

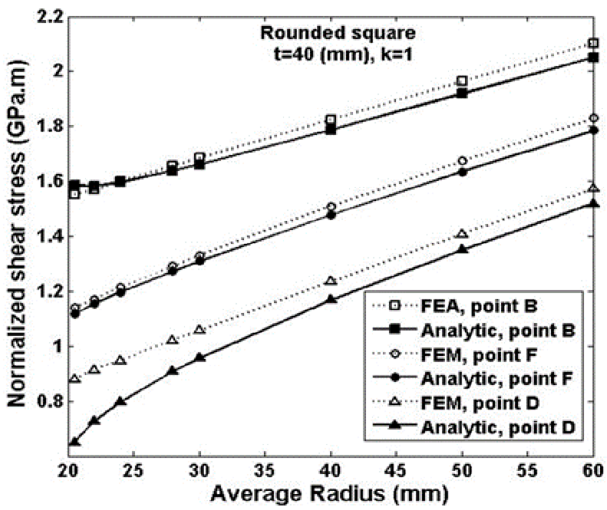

Fig. 11. Normalized shear stress at points D, F and B versus curvature radius with t=40 mm and k=1.

3.1.2 Flattened tube cross-section

Next, the effect of curvature radius on shear stress in a hollow shaft with a flattened tube cross-section is examined. The volume fraction parameter (k) is fixed as follows: 1. Thickness is considered the same in all parts of the cross-section. The effect of curvature radius on shear stress is evaluated for thicknesses of 5, 10, 20 and 40 mm.

The variation of the normalized shear stress at a flattened tube section with t=5 mm versus radius of curvature is investigated. The shear stress on the inner boundary at points A, E and C are shown in Fig. 12 and at points B, F and D of the outer boundary in Fig. 13. The hollow points in these figures show the results of the FE simulations and, the solid points show the analytical solutions.

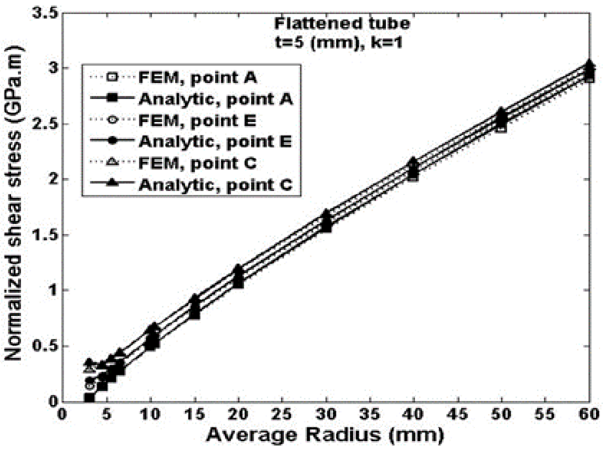

Fig. 12. Normalized shear stress at points C, E and A versus curvature radius with t=5 mm and k=1.

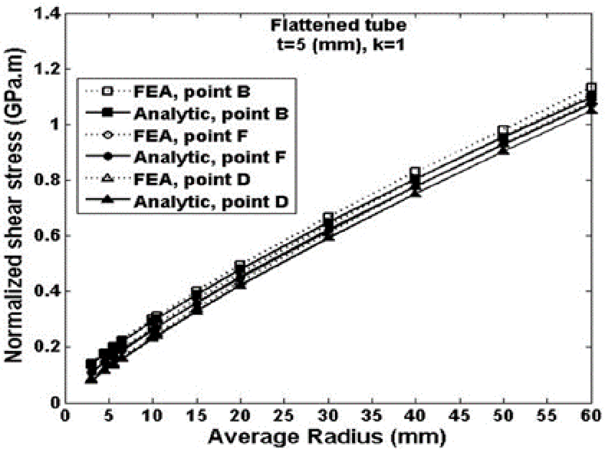

Fig. 13. Normalized shear stress at points D, F and B versus curvature radius with t=5 mm and k=1.

Accordingly, in the flattened tube cross-section with a constant thickness of 5 mm, the normalized shear stress obtained by both FE and the analytical methods, will have a uniform upward trend with an increase in the radius of curvature. On the other hand, there is a little difference between the FE and analytical results, except at the stress concentration region i.e., points C and E, where we have a difference of about 0.06 at R = 3 mm. Although this difference increases by increasing the curvature radius, it eventually reaches a value of 0.04, which is very low and negligible.

Considering the same conditions as the previous analysis, for the flattened tube cross-section with a thickness of 10 mm, the effect of changing the curvature radius on the normalized shear stress is investigated.

In the flattened tube cross-section with a thickness of 10 mm, the normalized shear stress has a uniform, increasing trend after increasing the radius of curvature, on all points of the inner boundary (Fig. 14) and those of the outer boundary (Fig. 15). Due to the stress concentrations at points C and E, the normalized shear stress for R=5 mm has a higher value than that of the next curvature, as shown in Fig. 14. The difference between analytical and FE results, is negligible at large curvatures. As the radius of curvature decreases, this difference increases and eventually, reaches a maximum value of 0.3 at point C for R=5.

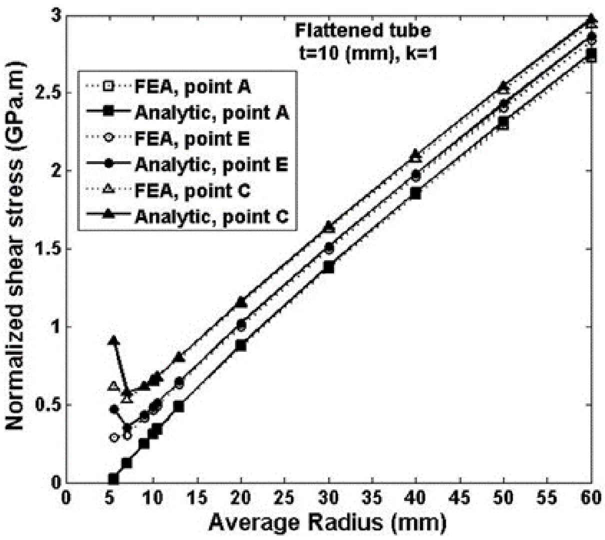

Fig. 14. Normalized shear stress at points C, E and A versus curvature radius with t=10 mm and k=1.

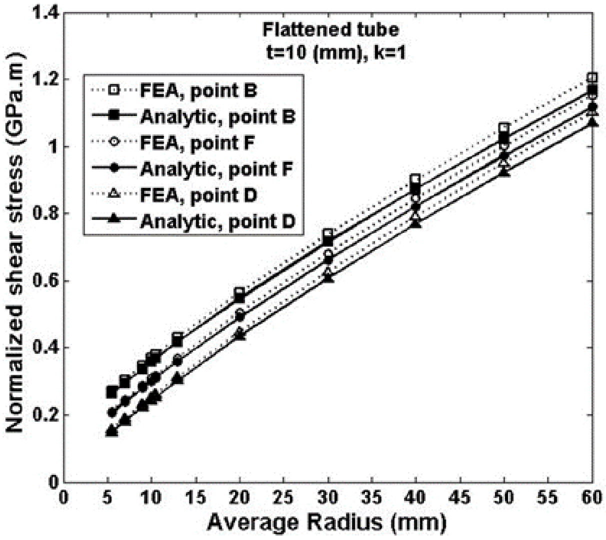

Fig. 15. Normalized stress at points D, F and B versus curvature radius with t=10 mm and k=1.

The results of the normalized shear versus curvature radius are shown in Figures 16 and 17 for the flattened tube cross-section with a thickness of 20 mm. The normalized shear stress at points B, F and D on the outer boundary and point A on the inner boundary obtains a uniform, increasing trend by increasing the curvature radius. However, at points E and C on the inner boundary, the shear stress has a decreasing trend up to R=12 mm, which is due to the stress concentration at these low curvature points. After this, the variation of the normalized shear stress returns to its usual ascending trend.

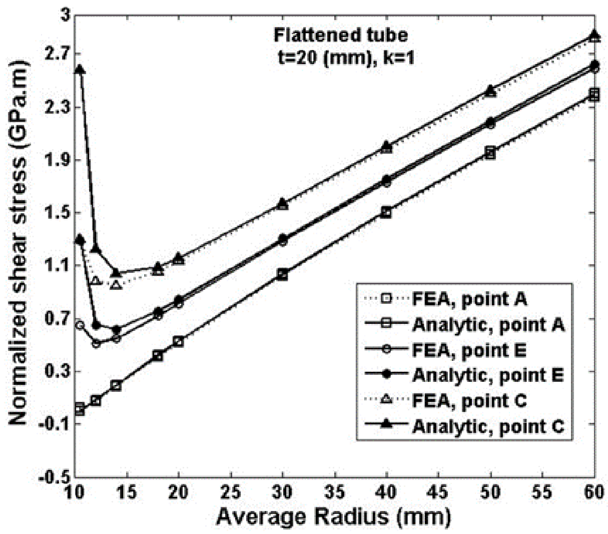

Fig. 16. Normalized shear stress at points C, E and A versus curvature radius with t=20 mm and k=1.

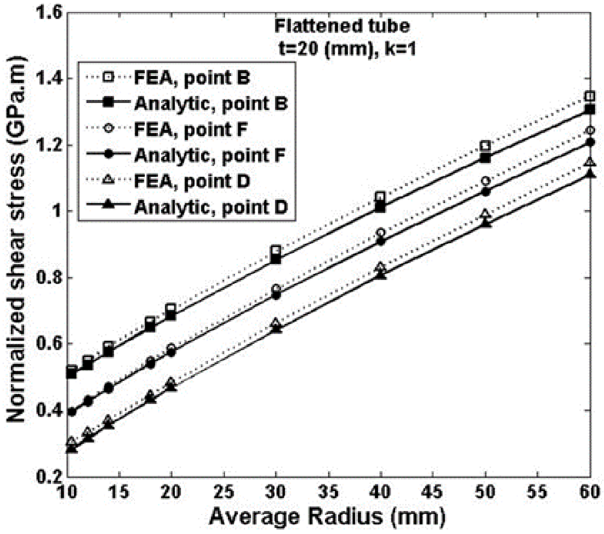

Fig. 17. Normalized shear stress at points D, F and B versus curvature radius with t=20 mm and k=1.

The difference between analytical and FE results, also increases by increasing the curvature radius. However, this difference is negligible, except at points C and E, where stress concentration exists. At points C and E, this difference gets the values of 1.3 and 0.7, respectively. Hence, a correction factor for the analytical formula should be applied at stress concentration regions.

Figures 18 and 19 show the stress analysis results for the flattened tube cross-section with a thickness of 40 mm. At all points on the inner boundary and point A on the inner boundary, the normalized shear stress increases by increasing curvature radius. At points E and C, up to R=28 mm, the normalized shear stress versus curvature radius has a decreasing trend due to the stress concentration. After that, the shear stress returns to the usual increasing trend as the stress concentration is removed.

By comparing the FE and analytical results at points E and C, a difference of 2.48 and 5.26 are recognized, respectively. This significant difference, which is due to the stress concentration, requires the implementation of SCFs to correct the analytical formula at stress concentration regions for 40 mm thickness.

Obviously, with the aim of the presented results in this section, it is easy to analyze the shear stress at different points of the FGM hollow tube with a flattened tube cross-section at a different radius of curvatures and thickness.

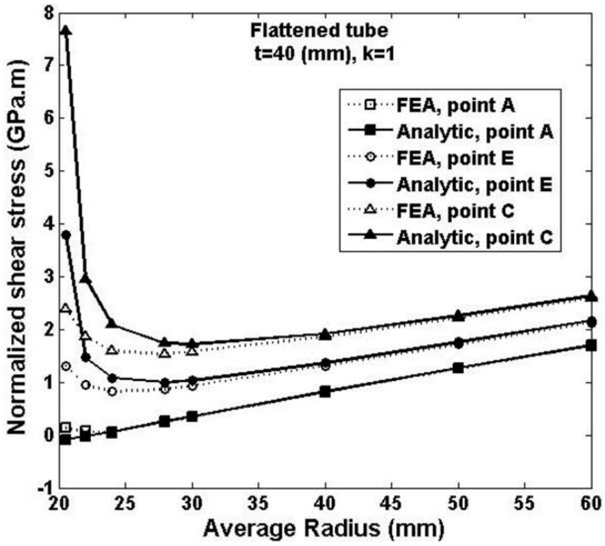

Fig. 18. Normalized shear stress at points C, E and A versus curvature radius with t=40 mm and k=1.

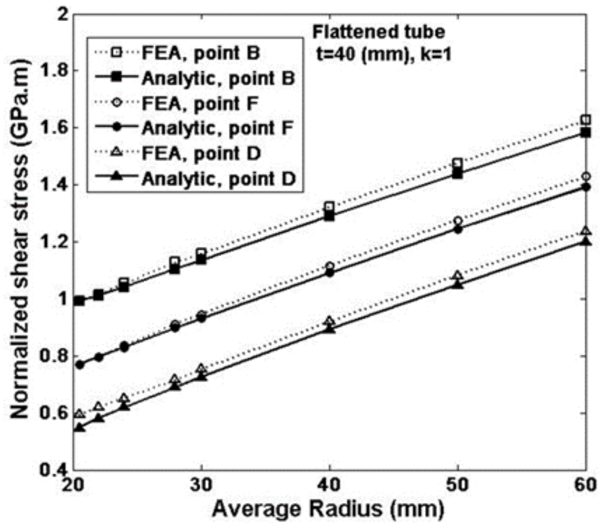

Fig. 19. Normalized shear stress at points D, F and B versus curvature radius with t=40 mm and k=1.

3.1.3. Evaluation of Fillet-Radius and Thickness Ranges for application of SCFs

According to previous results, significant differences exist between analytical and FE stresses at low fillet-radiuses of the FG hollow tube cross-sections. Therefore, implementation of SCFs is required at these stress concentration regions to correct the analytical formula. In this section, a range for the fillet-radius and thickness of the hollow tube cross-sections is proposed, in which the SCFs should be applied.

For a better understanding, the percentage of relative error of analytical formula point C, as the critical point of stress concentration, is summarized in Table 2 for different fillet-radius and thickness of the rounded square cross-section. Obviously, for r_1=0.5 to 10 mm, the relative error is high for larger thicknesses, i.e. t >5 mm. However, for t=5 mm and smaller thicknesses, if r_1<4 mm, then SCFs should be applied to analytical shear stresses.

Table 2. Error of the calculated analytical normalized shear stress at point C for rounded square cross-section

	Relative Error Percent (%)			
r_1 (mm)	t=5 mm	t=10 mm	t=20 mm	t=40 mm
0.5	40.804%	82.480	159.044	333.086
2	7.917 %	18.708	45.151	99.497
4	1.158	7.488	21.887	53.520
8	1.702	3.396	9.067	25.542
10	1.577	2.781	5.847	20.306
20	1.106	1.172	1.930	6.855
30	1.349	1.089	1.295	3.389
40	1.187	1.052	0.515	2.124
50	1.105	1.092	1.130	1.331

Similar investigations are performed for FG hollow tube with the flattened tube cross-section (Table 3). If $r_1 \leq 2$ mm, then for all thicknesses the SCFs should be used in analytical formula. For large thickness values, $t \geq 20$ mm, the stress correction factors are needed for $0.5 \leq r_1 \leq 8$ mm.

Table 3. Error of the calculated analytical normalized shear stress at point C for flattened tube cross-section

	Relative Error Percent (%)			
r_1 (mm)	t=5 mm	t=10 mm	t=20 mm	t=40 mm
0.5	20.633	47.596	99.110	219.151
2	2.346	8.371	24.711	58.894
4	1.197	0.232	9.381	31.252
8	0.050	1.255	2.985	14.238
10	0.522	1.241	1.172	8.244
20	1.099	1.147	1.162	2.614
30	1.100	1.112	1.129	1.640
40	1.372	1.101	1.112	1.357

According to the proposed ranges for fillet-radius and thickness of the FG cross sections, the SCFs are calculated and presented in Section 3.3.

3.2. Effects of FGM parameter variation across the section thickness on normalized shear stress

In this section, the effect of the nonlinear distribution of the FGM on plots of normalized shear stress versus curvature radius is investigated for a hollow tube with a constant cross-section thickness by performing FE simulations. The normalized shear stress values are evaluated for k=2,3,4 and five on both inner and outer boundaries of the proposed cross-section.

3.2.1 Rounded square cross-section

For a hollow FG tube with a rounded square cross-section of t=5 mm thickness, as shown in Fig. 20-22, the normalized shear stress has increased by increasing the curvature radius for all values of k. On the other hand, increasing the coefficient k decreases the amount of normalized shear stress at each curvature radius. By changing k=1 to k=5, the stress values will have a reduction of 4.4%, approximately.

According to Figures 21 and 22, at points E and C, the amount of shear stress decreases by increasing the value of k at all curvature radiuses. For example, at the minimum curvature radius, by changing k=1 to k=5, shear stress reductions of 8.7% and 10.9% are observed, at points C and E, respectively.

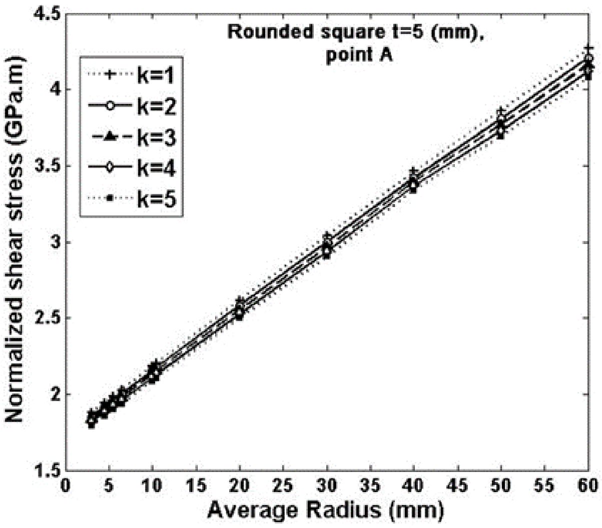

Fig. 20. Normalized shear stress at point A versus curvature radius with t=5 mm and variation of k.

It is worth noting that increasing the value of k, in the stress concentration regions, reduces the shear stress values and thus, the stress concentration, significantly. This fact can be used as a way to reduce the stress concentration at the desired FG hollow tube. Although the most considerable reduction in the present study is related to changing the value of k from one to five, the distance between the k=1 and k=2 plots is more significant. The plots for other values of k are almost in the same line.

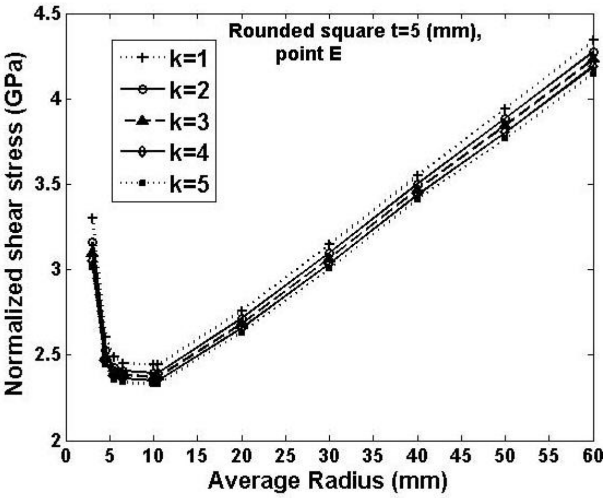

Fig. 21. Normalized shear stress at point E versus curvature radius with t=5 mm and variation of k.

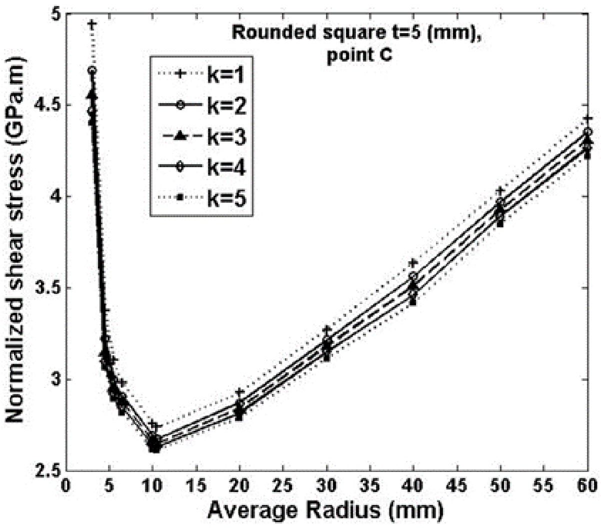

Fig. 22. Normalized shear stress at point C versus curvature radius with t=5 mm and variation of k.

3.2.2 Flattened tube cross-section

For the flattened tube cross-section with a constant thickness of 5 mm, according to Figures 23, 24 and 25, increasing the value of k reduces the amount of normalized shear stress at each curvature radius. The most significant reduction is accompanied by the change of linear distribution to the second degree, i.e., changing k=1 to k=2. Additionally, the distances between the plots of shear stress for different values of k, increase by increasing the curvature radius.

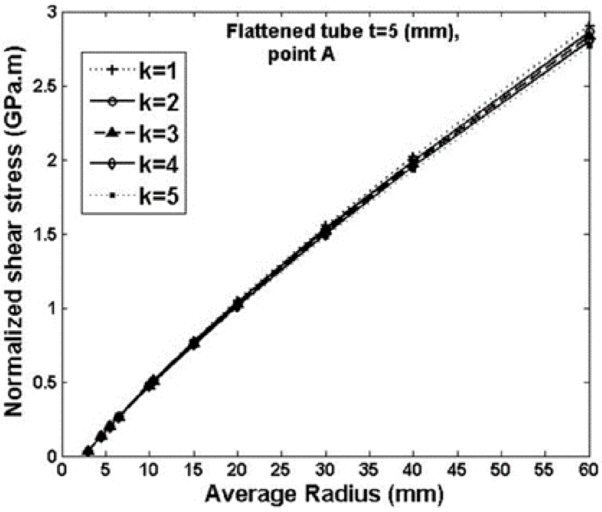

Fig. 23. Normalized shear stress at point A versus curvature radius with t=5 mm and variation of k.

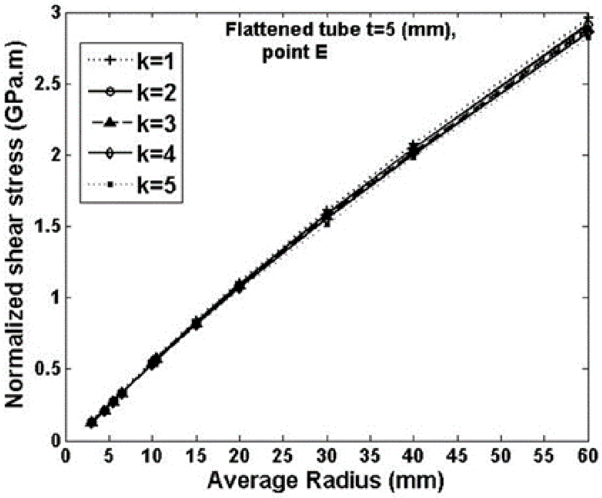

Fig. 24. Normalized shear stress at point E versus curvature radius with t=5 mm and variation of k.

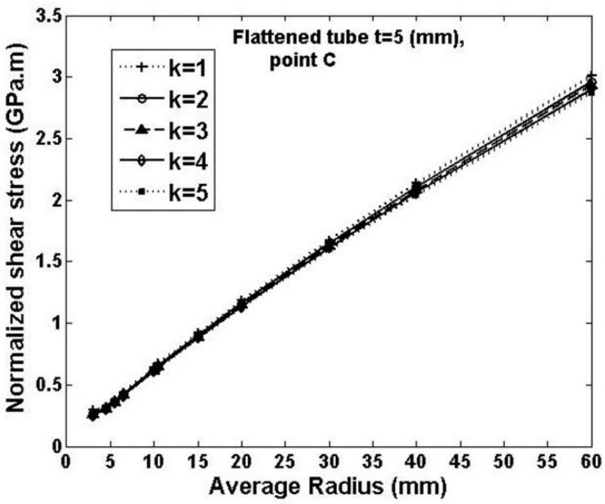

Fig. 25. Normalized shear stress at point C versus curvature radius with t=5 mm and variation of k.

3.3 Evaluation of the SCFs

As stated in Section 3.1, there is a difference between the shear stress values obtained by the analytical method and those of the FE simulations, due to the stress concentration in the low-curvature corners of the FGM hollow tube cross-sections. Therefore, to correct the analytical formula, some SCFs are presented here. Figure 26 (a) shows the SCFs for the rounded square cross-section and Figure 26 (b) shows those of the flattened tube cross-section. The SCFs versus curvature radius are obtained for different values of cross-section thickness.

As can be seen in Fig. 26, in each radius of curvature, by increasing the cross-section thickness, the difference between FE and analytical results gains a more considerable value and, the SCFs differ significantly from 1. Moreover, in each thickness, the stress concentration reduces by increasing the curvature radius and, the SCFs reach the value of 1.

With the aim of the presented results, the SCFs for other values of curvature radius can be obtained by interpolation. Consequently, using these SCFs, the analytical formula of Ref. [7], can also be applied to the stress concentration regions of both rounded square and flattened tube cross-sections made of FGMs., with reasonable accuracy.

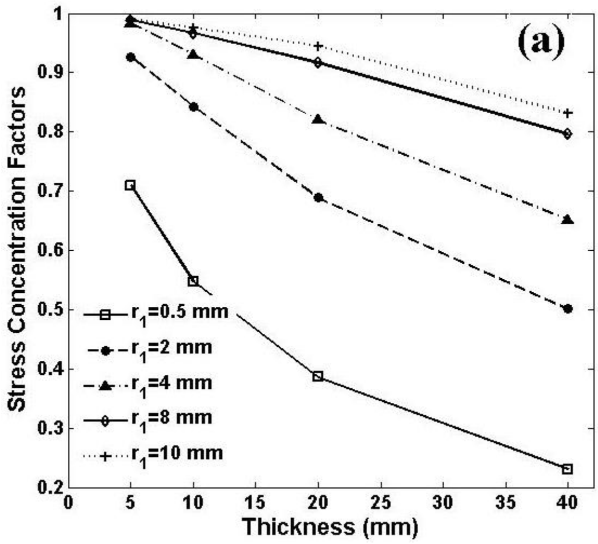

Fig. 26. The calculated SCFs. (a) Rounded square cross-section and, (b) flattened tube cross-section.

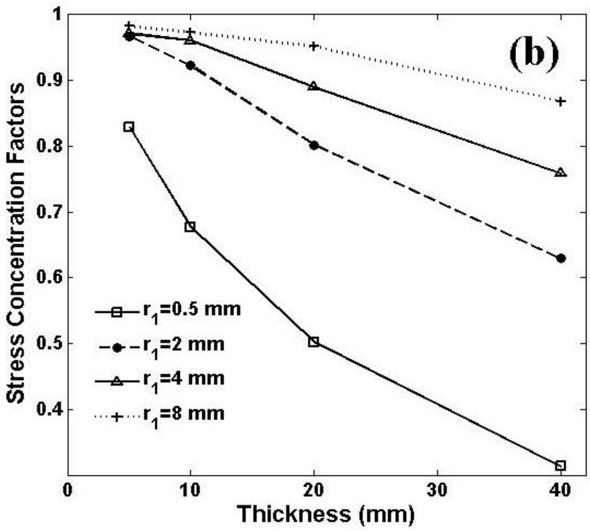

Fig. 26. Continue.

4. Conclusions

A FE model was developed to calculate SCFs of FG hollow tubes under torsion. The shear stresses in FG hollow tubes with curved edges were investigated for different curvature radiuses of the cross-section corners. The rounded square and flattened tube hollow bars were investigated. The plots of SCFs versus curvature radius of the corners were obtained for a variety of the cross-section thicknesses. The FE results are compared with results of a proposed analytical model.

With the aim of the presented results, SCFs for other values of curvature radius can be obtained by interpolation. Using these SCFs, the proposed analytical formula can also be applied to the stress concentration regions for FG hollow tubes with curved edge cross-sections with reasonable accuracy. The effects of constituent volume fractions were also investigated for a range of the radius of the curved segments.

5. References

[1] R. Chandra, A.D. Stemple, I. Chopra, Thin-walled composite beams under bending, torsional, and extensional loads. *Journal of Aircraft*, 27 (1991) 619-626.

[2] M. Savoia, N. Tullini, Torsional response of inhomogeneous and multilayered composite beams. *Composite Structures*, 25(1993) 587-594.

[3] C.O. Horgan, A.M. Chan, Torsion of functionally graded isotropic linearly elastic bars. *Journal of Elasticity*, 51(2) (1998) 181-199.

[4] G. Mejak, Optimization of cross-section of hollow prismatic bars in torsion. *Communications in Numerical Methods in Engineering*, 16(10) (2000) 687-695.

[5] M.R. Hematiyan, A. Doostfatemeh, Torsion of moderately thick hollow tubes with polygonal shapes. *Mechanics Research Communications*, 34 (2007) 528-537.

[6] A. Doostfatemeh, M.R. Hematiyan, S. Arghavan, Closed-Form Approximate Formulas for Torsional Analysis of Hollow Tubes with Straight and Circular Edges, *Journal of Mechanics*, 25 (2009) 401-409.

[7] I. Ecsedi, Some analytical solution for saint-venant torsion of non-homogeneous cylindrical bars, *European Journal of Mechanics-A/Solids*., 28(5) (2009) 985-990.

[8] S. Arghavan, S., M.R. Hematiyan, Torsion of functionally graded hollow tubes. *European Journal of MechanicsA/Solids*, 28 (2009) 551-559.

[9] B. Golami Bazehhour, J. Rezaeepazhand, Simplified approach for torsional analysis of non-homogenous tubes with non-circular cross-sections. *International journal of engineering*, 25(3) (2012) 277-287.

[10] Y. Bayat, M. Alizadeh, A. Bayat, Generalized solution of functionally graded hollow cylinder under torsional load. *journal jcarme*., 2(2) (2013) 23-32.

[11] A. Talebanpour, M.R. Hematiyan, Torsional Analysis of piezoelectric hollow bars. *International Journal of Applied Mechanics*., 6(02) (2014) 1450019.

[12] R. Barrettaa, R. Luciano, J.R. Willis, On torsion of random composite beams. *Composite structures*, 132 (2015) 915-922.

[13] I. Eshraghi, N. Soltani, M. Rajabi, Transient stress intensity factors of functionally graded hollow cylinders with internal circumferential cracks, *Latin American Journal of Solids and Structures*, 13 (2016) 1738-1762.

[14] R.C. Batra, G.J. Nie, Torsional deformations and material tailoring of orthotropic bi-directional FGM hollow truncated conical cylinders with curved lateral surfaces. *International Journal of Engineering Science*, 133 (2018) 336–351.

[15] G. Wang, L. Dong, and S.N. Atluri, Direct and inverse multi-scale analyses of arbitrarily functionally graded layered hollow cylinders (discs), with different shaped reinforcements, under harmonic loads. *Composite Structures*, 188 (2018) 425–437.

[16] A. Ghassemi, M. Noroozi, Torsion analysis of infinite hollow cylinders of functionally graded materials weakened by multiple axisymmetric cracks, *Theoretical and Applied Fracture Mechanics*, 96 (2018) 811-819.

[17] S. Nikbakht, S. Kamarian, M. Shakeri, A review on optimization of composite structures Part II: Functionally graded materials, *Composite Structures*, 214 (2019) 83–102.

[18] V. Nigrelli, G.V. Mariotti, Stress concentration factor in collar and shouldered shafts in torsion, *Engineering Analysis with Boundary Elements*, 16 (1995) 71-77.

[19] M.T. Ozkan, F. Erdemir, Determination of stress concentration factors for shafts under tension, Materials Testing, 62(4) (2020) 413-421.